Title

High-resolution imaging reveals indirect coordination of opposite motors and a role for LIS1 in high-load axonal transport

Journal

Journal of Cell Biology, 195(2)

ISSN

0021-9525

Authors

Yi, Julie Y
Ori-McKenney, Kassandra M
McKenney, Richard J
et al.

Publication Date

2011-10-17

DOI

10.1083/jcb.201104076

Peer reviewed

High-resolution imaging reveals indirect coordination of opposite motors and a role for LIS1 in high-load axonal transport

Julie Y. Yi,[1] Kassandra M. Ori-McKenney,[1] Richard J. McKenney,[1] Michael Vershinin,[2] Steven P. Gross,[3] and Richard B. Vallee[1]

[1]Department of Pathology and Cell Biology, Columbia University, New York, NY 10027
[2]Department of Physics and Astronomy, University of Utah, Salt Lake City, UT 84112
[3]Department of Developmental and Cell Biology, University of California, Irvine, Irvine, CA 92697

The specific physiological roles of dynein regulatory factors remain poorly understood as a result of their functional complexity and the interdependence of dynein and kinesin motor activities. We used a novel approach to overcome these challenges, combining acute in vivo inhibition with automated high temporal and spatial resolution particle tracking. Acute dynein inhibition in nonneuronal cells caused an immediate dispersal of diverse forms of cargo, resulting from a sharp decrease in microtubule minus-end run length followed by a gradual decrease in plus-end runs. Acute LIS1 inhibition or LIS1 RNA interference had little effect on lysosomes/late endosomes but severely inhibited axonal transport of large, but not small, vesicular structures. Our acute inhibition results argue against direct mechanical activation of opposite-directed motors and offer a novel approach of potential broad utility in the study of motor protein function in vivo. Our data also reveal a specific but cell type–restricted role for LIS1 in large vesicular transport and provide the first quantitative support for a general role for LIS1 in high-load dynein functions.

Introduction

The major form of cytoplasmic dynein, dynein 1, is responsible for transport of membrane vesicles and macromolecular cargoes at micrometer/second rates. Cytoplasmic dynein is also involved in transport and positioning of large cargoes, such as nuclei, chromosomes, and the mitotic spindle (Faulkner et al., 2000; Shu et al., 2004; Tanaka et al., 2004; Siller et al., 2005; Tsai et al., 2005; Grabham et al., 2007; Stehman et al., 2007; Vergnolle and Taylor, 2007). Recruitment of dynein to diverse subcellular structures has been ascribed to a variety of factors, two of which have also been implicated in dynein motor regulation: dynactin, which is reported to increase dynein processivity in in vitro biophysical assays (King and Schroer, 2000; Culver-Hanlon et al., 2006; Ross et al., 2006; Kardon et al., 2009), and LIS1, which, along with nuclear distribution gene E (NudE) and NudE like (NudEL), adapts cytoplasmic dynein for sustained force generation (McKenney et al., 2010).

Several studies have addressed the effects of dynein inhibition and that of its regulatory cofactors in vivo, but interpretation has been complicated by evidence for reciprocal inhibition of microtubule plus-end– and minus-end–directed motors (Brady et al.,1990; Waterman-Storer et al., 1997; Martin et al., 1999; Pilling et al., 2006; Kim et al., 2007; Barkus et al., 2008; Shubeita et al., 2008; Bremner et al., 2009; Uchida et al., 2009). Although this effect has obscured the detailed contributions of individual motors to particle motility, it has received attention as evidence for mechanical coordination of opposite-directed motor activities (Müller et al., 2008; Ally et al., 2009).

The current study was initiated to define conditions under which dynein-specific inhibitory effects could be discerned and to apply this approach to resolving the role of LIS1, in particular, in vesicular transport. We previously found LIS1 to be recruited

Correspondence to Richard B. Vallee: rv2025@columbia.edu

K.M. Ori-McKenney's present address is Dept. of Cellular and Molecular Pharmacology, University of California, San Francisco, San Francisco, CA 94102.

R.J. McKenney's present address is Dept. of Cellular and Molecular Pharmacology, University of California, San Francisco, San Francisco, CA 94102.

Abbreviations used in this paper: DN, dominant negative; LE, late endosome; MSD, mean square displacement.

The Rockefeller University Press $30.00
J. Cell Biol. Vol. 195 No. 2 193–201
www.jcb.org/cgi/doi/10.1083/jcb.201104076

by NudE and NudEL to form a triple complex with dynein (McKenney et al., 2010). LIS1 interacted with the dynein motor domain during its power stroke to prolong the interaction of dynein with microtubules and increase the total force generated by multiple dynein molecules (McKenney et al., 2010). These results identify a role for LIS1 in high-load aspects of cytoplasmic dynein function, which is consistent with its requirement in nuclear and centrosome transport, chromosome dynamics, and spindle orientation (Faulkner et al., 2000; Dujardin et al., 2003; Shu et al., 2004; Tanaka et al., 2004; Tsai et al., 2005, 2007, 2010). An involvement for LIS1 in low-load transport, e.g., of membrane vesicles, has been controversial, despite a contribution of NudEL in this behavior (Zhang et al., 2009). LIS1 dominant negatives (DNs) severely inhibited mitosis and cell migration, with no detectable effect on lysosome, endosome, or Golgi distribution (Faulkner et al., 2000; Tai et al., 2002; Dujardin et al., 2003). However, LIS1 overexpression caused Golgi compaction (Smith et al., 2000), and LIS1 RNAi was reported to disperse a variety of vesicular organelles (Lam et al., 2010). Endosomes also accumulate at hyphal tips in *Aspergillus* LIS1 deletion mutants (Zhang et al., 2010). The implications of these disparate results for LIS1 function in vesicular transport remain an important unresolved issue.

To address the specific roles of dynein and its regulators in vivo, we have combined acute inhibition with high-resolution particle tracking. We observed specific interference with minus-end microtubule vesicular motility immediately after acute dynein inhibition, arguing against direct mechanical coupling with kinesins. We saw little effect of acute LIS1 inhibition in non-neuronal cells but detected a dramatic rapid-onset block in axonal transport of large, but not small, membranes. These results identify differential requirements for LIS1 in vesicular transport depending on subcellular environment and support a role in high-load functions.

Results and discussion

Rapid dispersal of cargoes in acutely dynein-inhibited cells

To test the effects of acute dynein inhibition on subcellular cargos, we injected several purified function-blocking reagents into live COS-7 cells. Immediately after injection of a dynein function-blocking monoclonal antibody (74.1 Ab), the majority of LysoTracker-positive lysosomes/late endosomes (LEs; lysos/LEs) redistributed en masse toward the cell periphery. Rapid long-range centrifugal movements were initially evident (Figs. 1 A and S1 C; see Video 1 vs. Video 2 for IgG control), although by 10 min, the fraction of stationary particles had increased (~60% at 10 min vs. ~30% at 1 min; Figs. 1 A and 2 D). A similar pattern of rapid dispersal followed by an overall reduction in motility was observed for another lyso/LE marker, GFP-NPC1 (25 cells showing dispersal phenotype/25 total), and markers for early endosomes (25/25), Golgi elements (30/30), and fluorescently labeled adenovirus (40/40; Figs. 1 B and S1 E). We observed similar effects on lysos/LEs using the 70.1 anti-dynein antibody (18/18) and a function-blocking anti-NudE/NudEL (NudE/L) antibody (19/19 cells; Stehman et al., 2007) as well as the DN dynactin CC1 fragment (5/5; Fig. 1 C). No apparent effect was observed using an antibody to the dynactin p150^{Glued} cytoskeleton-associated protein–Gly microtubule-binding domain (seven cells showing no dispersal phenotype/seven total), a function-blocking anti-LIS1 N-terminal antibody (5/5; Faulkner et al., 2000), or a DN N-terminal LIS1 fragment (28/28; Tai et al., 2002) expressed in *Escherichia coli* (Figs. 1 D and S1 D). The latter results were despite severe effects of the antibody on mitotic progression (Faulkner et al., 2000). We also found overnight incubation of cells injected with the N-terminal fragment to cause arrest in mitosis (27/35 cells; Fig. S1 A). Similar effects of 74.1 Ab on lysos/LEs were obtained in HeLa-M, A549, and GFP-Lamp1–expressing COS-7 cells (Fig. S1 B).

High-resolution particle tracking in dynein and LIS1-inhibited cells

To gain further insight into changes in motor protein activity underlying these results, we imaged lysos/LEs in live COS-7 cells at ~17 frames/s for 1 min at 1, 5, and 10 min (Videos 3, 4, and 5, respectively) after acute inhibition and analyzed the data by automated particle tracking (Bremner et al., 2009; Ori-McKenney et al., 2010). In uninjected controls (Fig. 2 A, left), linear particle movements in the microtubule minus- or plus-end direction were punctuated by stops and abrupt or gradual reversals, the latter consistent with tug-of-war events between plus and minus motors (Soppina et al., 2009).

By 1 min after injection of the 74.1 anti-dynein antibody, a dramatic shift of net particle displacement in the microtubule plus-end direction was seen, which is consistent with our initial low-resolution observations (Fig. 1 A). The 74.1 Ab injection caused long plus-end travel events, which were interrupted by a pause or a short minus run followed by immobility (Figs. 2 A [middle left] and S2 B). These changes were associated with a sharp drop in minus-end–directed (Fig. 2 B, left) but not plus-end–directed run length (Fig. 2 B, right). Plus-end run length did decrease gradually with time (Fig. 2 B, right), as did the overall percentage of moving particles (see Materials and methods; Fig. 2 C), mean square displacement (MSD; Fig. 2 D), and net particle displacement (Fig. 2 E). No clear effect was observed on particle velocity (Fig. 2 F), the frequency of plus and minus runs, or the frequency of directional switching during the period of observation (not depicted).

LIS1 inhibition produced no apparent effect on overall lyso/LE distribution (Fig. 1 D and Video 6) or on lyso/LE run length either in the minus- or plus-end directions (Fig. 2 B), percentage of motile particles (Fig. 2 C), MSD (Fig. 2 D), net displacement (Fig. 2 E), and velocity, except for a slight increase of plus velocity at 5 min (Fig. 2 F). However, we did detect a moderate increase in an oscillatory form of behavior consisting of repetitive, short bidirectional linear movements (Fig. 2 A, right). These movements were typically collinear and <2–3 µm in magnitude.

Role of LIS1 in axonal transport

This behavior suggested an inability of lysos/LEs to overcome some form of resistance to their transport under LIS1 inhibitory conditions. To test this possibility in confined cytoplasmic

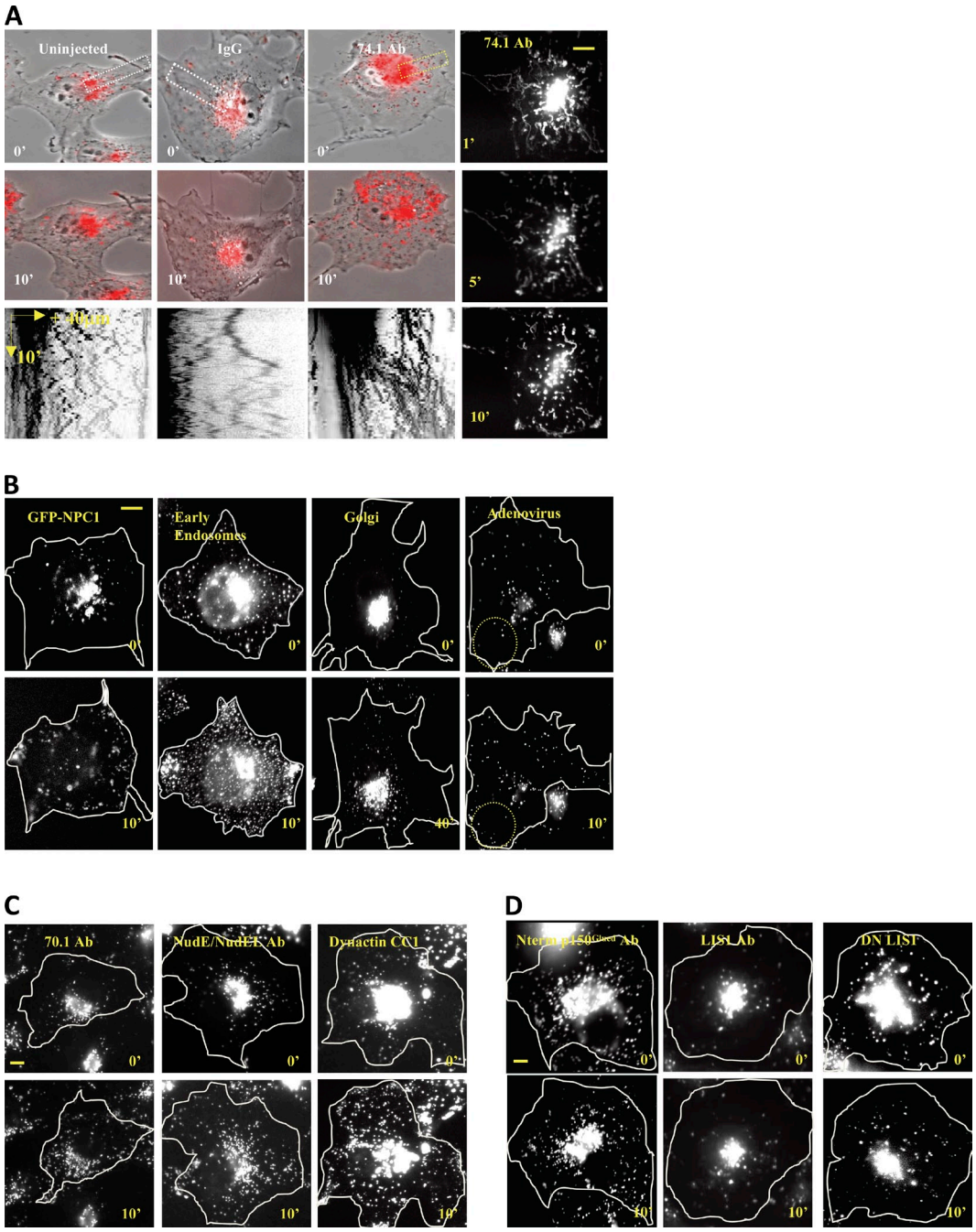

Figure 1. **Rapid dispersal of organelles by acute dynein inhibition.** Lysos/LEs rapidly redistribute to the cell periphery by 74.1 Ab microinjection in COS-7 cells within 10 min after injection. (A) Uninjected, IgG, and 74.1 Ab–injected cells are shown at 0 and 10 min after injection. The rightmost panels are time projection images at 1, 5, and 10 min after injection. Kymographs of the indicated regions (dotted rectangles) are shown in the bottom row. Only the 74.1 Ab–injected cell showed en masse lysosome dispersal as shown in the kymograph as plus-biased motion. (B) GFP-NPC1, Rab5-GFP (early endosomes), *N*-acetylglucosaminyltransferase–GFP (Golgi), and adenovirus Alexa Fluor 546 were dispersed. Dotted circles denote dispersed particles. (C) LysoTracker-positive particles were also dispersed by 70.1 Ab, NudE/L antibody, and the purified CC1 fragment of the $p150^{Glued}$ dynactin protein. (D) N-terminal $p150^{Glued}$ dynactin antibody, function-blocking LIS1 antibody, and DN LIS1 protein did not affect overall lysosome distribution. All images were taken immediately after injection (0 min) and after 10 min postinjection unless specified otherwise. Bars, 10 µm.

regions and to understand more completely the effects of LIS1 inhibition in the central nervous system, we used cultured rat cortical neurons. Lysosomal transport has been reported to be reduced by NudEL inhibition in neuronal (Zhang et al., 2009) and nonneuronal cells, but the extent to which these effects involve LIS1 and the detailed consequences for cargo behavior are unknown.

Lysos/LEs in uninjected rat cortical neurons showed predominantly retrograde transport (Fig. 3 A and Video 7), which was strongly inhibited by the 74.1 (Fig. 3 A and Video 8) and anti-NudE/L antibodies (Figs. 3 [A and C] and S3 C and Video 9). The effect was not as immediate as in nonneuronal cells, probably in part reflecting the greater distance required for antibody diffusion along the axon. Plus-end transport persisted at some level in most

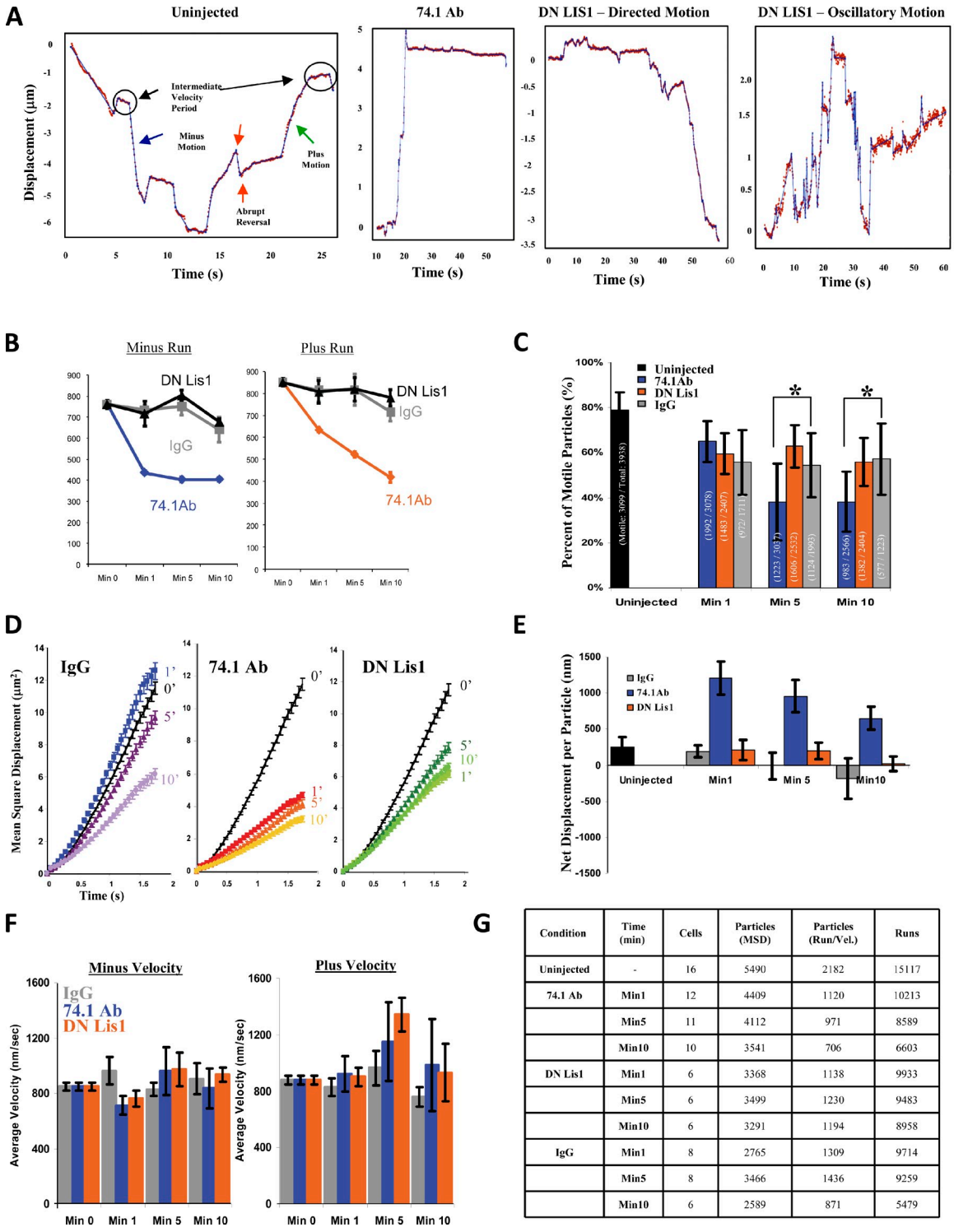

Condition	Time (min)	Cells	Particles (MSD)	Particles (Run/Vel.)	Runs
Uninjected	-	16	5490	2182	15117
74.1 Ab	Min1	12	4409	1120	10213
	Min5	11	4112	971	8589
	Min10	10	3541	706	6603
DN Lis1	Min1	6	3368	1138	9933
	Min5	6	3499	1230	9483
	Min10	6	3291	1194	8958
IgG	Min1	8	2765	1309	9714
	Min5	8	3466	1436	9259
	Min10	6	2589	871	5479

Figure 2. **High-resolution lyso/LE particle–tracking analysis in COS-7 cells.** High-temporal resolution recordings (~17 frames/s) of lyso/LE motion were processed for analysis. (A) Examples of lysosomal tracks from an uninjected cell showing normal bidirectional lyso/LE motility, a 74.1 Ab–injected cell showing long plus-end–directed travel, and LIS1 DN–injected cells showing normal minus-end–directed transport and oscillatory movement (also see Fig. S2 B). (B–G) Effect of 74.1 and DN LIS1 injection on COS-7 cell lyso/LE motility. Run length (B), percentage of motility (C), and MSD (D) are shown. (E) Net displacement/particle (= [Σ-plus runs (nm) − Σ-minus runs (nm)]/number of particles). (F) Average particle velocity is shown. All error bars represent SEM. *, $P < 0.05$. (G) Sample size for particle-tracking analysis.

cells throughout the initial 10-min observation period (unpublished data) in contrast to the effects observed in COS-7 cells, suggesting less plus–minus coupling in neurons. The end result of the 74.1 injection was a substantial shift to plus-end movements. However, in cells injected with anti-NudE/L antibody, bidirectional movement of small particles persisted (Fig. 3 C, orange arrows).

Injection of anti-LIS1 antibody potently inhibited lyso/LE behavior in neurons but in a manner distinct from that for

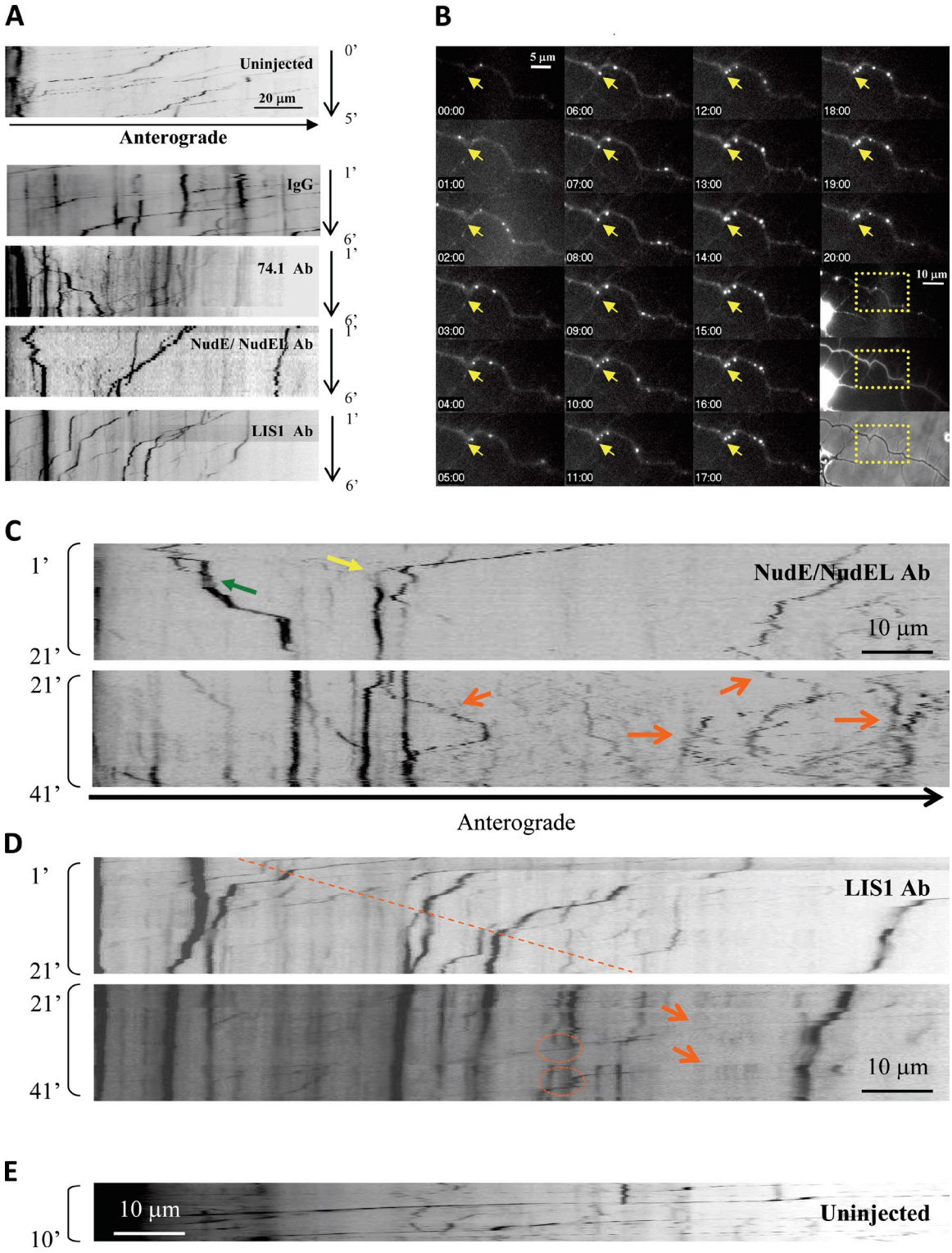

Figure 3. **Differential lysosomal motility inhibition phenotypes induced by NudE/L and LIS1 inhibition in neurons.** Lysos/LEs in rat cortical neurons showed mostly retrograde transport in uninjected and IgG controls, whereas severe inhibition was observed with 74.1 Ab, NudE/L antibody, and LIS1 antibody–injected cells. (A) Kymographs showing cells 1–6 min after injection. Arrest of several large particles is observed by 6 min in LIS1 antibody–injected cells. (B) Time-lapse images of the same LIS1 antibody–injected cell showing large lysosome arresting at the axonal kink (yellow arrow). Boxed areas show LysoTracker red versus dextran fluorescence versus phase-contrast images of the region shown. (C and D) Long-duration videos of the same LIS1 antibody–injected axon and a NudE/L antibody–injected axon. Note the near-complete arrest of motility in the LIS1 antibody–injected case by 20 min as opposed to continued bidirectional motility in the NudE/L antibody–injected case. Note the severe arrest (yellow arrow) as well as the directional reversal (green arrow) in the first 20 min after injection using anti-NudE/L antibody but the extensive bidirectional movement persistent beyond 20 min (orange arrows in C). Lysos/LEs in LIS1 antibody–injected cells showed progressive linear arrest with distance from the cell body (dotted line) during the first 21 min after injection, which is consistent with the diffusion of the antibody along the axon. Although larger particles remained immobile, smaller particles showed rapid transport (orange arrows in D) and could bypass the larger particles (dotted circles). (E) In control cells, lysos/LEs moved mostly in retrograde direction. Kymographs were generated from as near the cell body as imaging could be performed to up to 140 μm away.

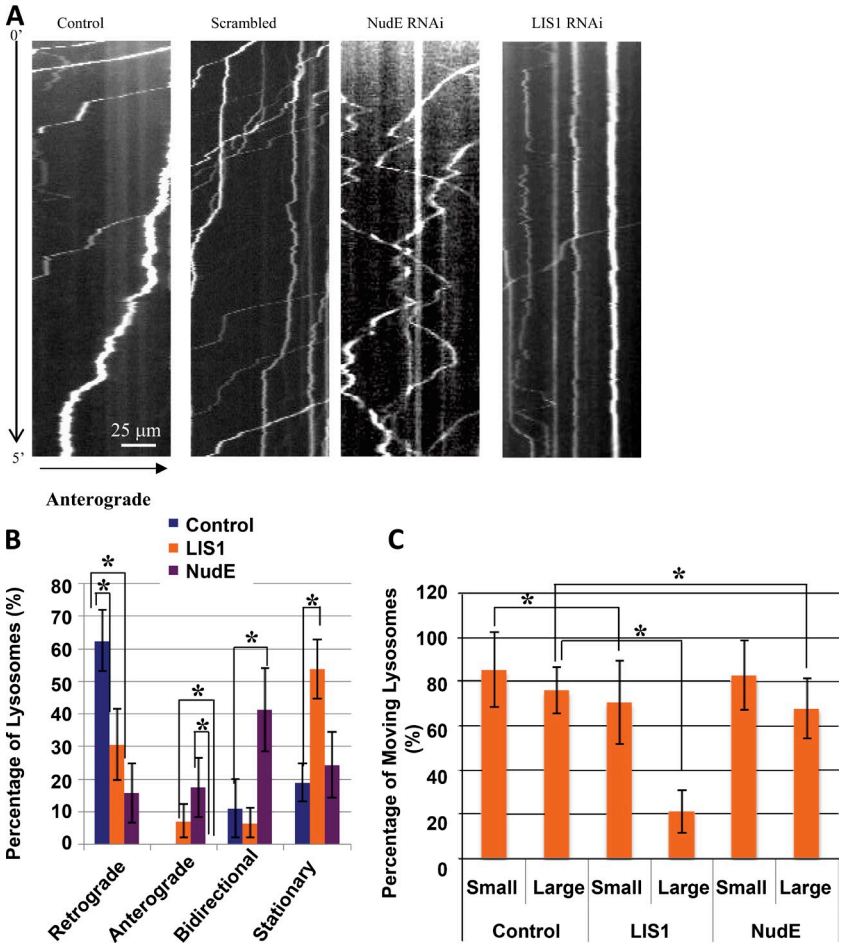

Figure 4. **Knockdown of NudE and LIS1 resembles acute inhibitions.** (A) Lysos/LEs in rat hippocampal neurons moved mostly in the retrograde direction in wild-type and scrambled RNAi controls, but an increase in bidirectionally moving lysosomes and severe immobility of larger lysosomal particles (≥1 µm in diameter) were apparent in NudE RNAi and LIS1 RNAi cells, respectively. (A–C) Consistent with the NudE/L antibody–injected case, knockdown of NudE caused an increase in bidirectionally moving lysos/LEs (A and B), whereas knockdown of LIS1 protein more severely interfered with mobility of larger particles than smaller ones, which is consistent with the LIS1 antibody–injected case (A–C). Stationary, anterograde/retrograde, and bidirectional particles were defined as particles that displaced $|\Delta X| < 1$ µm, >5 µm in one direction, and >3 µm in both directions, respectively. The error bars represent SD (*, $P < 0.001$). The number of particles analyzed are as follows: control (small), $n = 60$; control (large), $n = 55$; LIS1 RNAi (small), $n = 40$; LIS1 RNAi (large), $n = 66$; NudE RNAi (small), $n = 46$; and NudE RNAi (large), $n = 38$ (using 10 axons per condition).

cytoplasmic dynein. Over a period of 1–41 min after injection, larger lysos/LEs (≥1 µm based on fluorescence pixel number normalized to phase-contrast dimensions; Fig. S3 A) showed gradual arrest (Fig. 3 [A and D] and Video 10), whereas a significant percentage of smaller particles continued to move actively, some clearly in the immediate vicinity of nonmotile large particles (Fig. 3 D, dotted circles). The inhibitory effect on the larger lysos/LEs advanced progressively away from the cell body region with time after injection (Fig. 3 D, dashed line), consistent with diffusion of the antibody through the axonal process. By 10–20 min, most of the large particles were arrested (Fig. 3 D) versus controls (Fig. 3 E), in which few such particles were stopped.

As a control for these observations and to increase sample size, we also performed NudE and LIS1 RNAi in hippocampal neurons. The results were strikingly similar to those from antibody injection. Again, NudE RNAi caused a pronounced shift from retrograde to bidirectional movement (Fig. 4, A and B), whereas LIS1 RNAi caused substantial particle arrest. Nonetheless, as for LIS1 antibody injection, neurons subjected to LIS1 RNAi showed persistent transport of small vesicles (Fig. 4, A–C).

Collectively, our results shed new light on the coordinate behavior of motor proteins and the role of LIS1, in particular, in dynein regulation. By acute inhibition of cytoplasmic dynein and its regulators, we could monitor the immediate consequences of altered motor behavior. Our results support coordinate inhibition of opposite-directed motor proteins (Kim et al., 2007; Ally et al., 2009; Bremner et al., 2009), which we now find to occur within several minutes of motor inhibition but not immediately. Instead, acute dynein inhibition has a specific effect on minus-end transport, providing a direct physiological readout of individual motor behavior. The more gradual decrease in plus-end transport argues against a role for direct mechanical activation of opposite-directed motors (Ally et al., 2009) in our system. The mechanism responsible for the gradual decrease in plus-end transport is unknown. Conceivably, plus-end–directed vesicles may run off their microtubule tracks or run into the cell cortex. Alternatively, dynein inhibition may activate a global cellular mechanism for down-regulating transport, the nature of which remains obscure.

We find the effect of LIS1 inhibition to be extremely limited in nonneuronal cells but very pronounced in neurons. We saw no effect of LIS1 inhibition on vesicular distribution in COS-7 cells, which is consistent with our earlier studies (Faulkner et al., 2000; Tai et al., 2002), though we observed a small increase in localized oscillatory behavior by lysos/LEs in the current study. This behavior may represent a partial version of the more complete arrest we observed for large vesicles in LIS1-inhibited neurons. In fact, NudE RNAi, which produces a generally weaker inhibitory effect than LIS1 inhibition, also caused pronounced particle oscillations of somewhat larger magnitude in hippocampal neurons (Fig. 4, A and B).

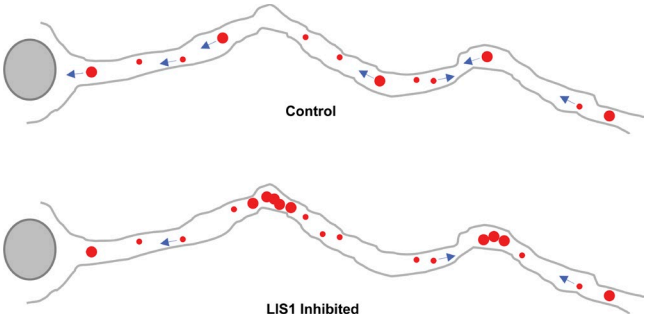

Figure 5. **Effect of LIS1 inhibition on lyso/LE transport in neurons.** Control hippocampal and neocortical neurons exhibited rapid lysos/LEs mostly in the retrograde direction. LIS1 inhibition specifically and potently blocked movement of large lysos/LEs, especially at axonal bends and branch points, with little effect on the smaller vesicular transport. These effects were not observed in nonneuronal cells, which is consistent with a role for LIS1 in transport under higher resistance conditions. Red dots indicate lyso/LE particles. Blue arrows indicate transport directions.

Inhibition of LIS1, and less so that of NudE or NudEL, preferentially affected larger, brighter lysos/LEs. These results provide the first direct quantifiable evidence for differential roles for LIS1 on the basis of cargo size. They may also help to reconcile evidence for misdistribution of endosomes in *Aspergillus* LIS1 (*NudF*)-null cells, the cytoplasm of which could have a high resistance to vesicular transport (Zhang et al., 2010). We observed strikingly similar effects of acute and longer-term LIS1 inhibition, indicating that arrest of larger particles is a direct consequence of altered dynein activity rather than an indirect effect of altered membrane trafficking. We did observe occasional coalescence of small vesicles to immotile aggregates, but most of the larger lyso/LEs arrested independently within minutes of acute LIS1 inhibition. We have recently demonstrated that NudE-LIS1 and dynactin compete with each other for binding to dynein in vitro (McKenney et al., 2011). This suggests that individual dyneins in vivo are subject either to NudE-LIS1 or dynein regulation but not both, which may be part of a novel mechanism to assign individual dyneins for specific modes of motor regulation and may play a role in the effects described here.

Together, our results support a requirement for LIS1 in high-load forms of dynein transport. We argue that the large lysos/LEs must be under LIS1 control even when traveling at high rates. This observation has the important consequence that LIS1 must be continuously active during high-speed stepping of dynein along the axonal microtubules. The nature of the resistance encountered by the larger lysos/LEs in our study is uncertain but likely involves local cytoplasmic constrictions, obstructions, or regions of higher viscosity (Figs. 3 B and 5). In this view, oscillations could reflect repeated efforts to bypass these impediments. The extent to which microtubule plus-end–directed kinesins contribute to these behaviors also remains to be explored further. Our results identify a novel conditional role for LIS1 in axonal transport. Mutations in cytoplasmic dynein, which affect vesicular transport, also result in neurodegeneration (Ori-McKenney et al., 2010). Whether similar effects will be found for the LIS1 gene remains an important issue for further investigation.

Materials and methods

Cells, antibodies, and protein purification

COS-7, A549, and HeLa-M cells (provided by V. Allan, University of Manchester, Manchester, England, UK) were grown in DME supplemented with 10% FBS. Primary hippocampal and cortical neurons (provided by S. Kemal, Columbia University, New York, NY) were obtained from E-18 or -19 rat embryonic brains and cultured in Neurobasal medium supplemented with L-glutamine and B-27 (Invitrogen) and incubated in 37°C with 2% CO_2 for at least 3 d to allow proper axon formation. To ensure free diffusion of injection reagents in axons, we only used cortical neurons from 3 or 4 d in vitro before formation of macromolecule gating filters in the initial segment of an axon (Song et al., 2009). The antibodies used for microinjection included affinity-purified 74.1 and 70.1 (Sigma-Aldrich) dynein intermediate chain antibodies, LIS1 antibody, dynactin p150^{Glued} cytoskeleton-associated protein–Gly antibody (BD), and IgG-cut NudE/L antibody (Stehman et al., 2007). Rat p150^{Glued}-CC1-FLAG (aa 223–530) and African green monkey N-terminal LIS1 (aa 1–87) fragments were cloned into pGEX6P vectors for bacterial expression and purified by glutathione affinity chromatography. Additional antibodies included rabbit/chicken anti-GFP (Invitrogen), rat anti-tyrosinated tubulin (Millipore), and rabbit anti-Lamp1 (Abcam).

Microinjection and live-cell imaging

For live-cell imaging experiments, cells were plated on uncoated glass-bottomed dishes for COS-7 cells (MatTek Corporation) and poly-L-lysine– and laminin-coated glass-bottom dishes for primary hippocampal and cortical neurons. For antibody injection, purified IgGs were concentrated in microinjection buffer (10 mM Hepes, pH 7.4, containing 140 mM KCl) to the following: 1 mg/ml monoclonal anti-dynein IC 74.1 and 1 mg/ml 70.1 (Sigma-Aldrich), 7 mg/ml polyclonal anti-NudE/L (Stehman et al., 2007), and 1 mg/ml anti–N-terminal p150^{Glued} (BD) or 1 mg/ml anti-LIS1 antibodies (Faulkner et al., 2000). Purified proteins for injection were concentrated in the same buffer as the antibodies to the CC1 fragment of p150^{Glued} dynactin (2 mg/ml) and N-terminal LIS1 (2 mg/ml; Tai et al., 2002). For control, 1 mg/ml rabbit IgG was prepared and concentrated in the same buffer as other samples. The final concentration of each sample was estimated by Bradford assay. Microinjections were performed with primary cultured neurons in neuronal culture medium (Neurobasal medium, L-glutamine, and B-27) and COS-7 cells in CO_2-independent recording media (Invitrogen) at 37°C with and without 2% CO_2, respectively. Success rates for injecting neurons were much lower than for nonneuronal cells. Rates of diffusion in neurons were estimated by injection of fluorescent dyes (Grabham et al., 2007) and Alexa Fluor 488 dextran (in this study). For RNAi experiments, neuronal cultures were transfected with LIS1, NudE, or scrambled RNAi by use of either Effectene (QIAGEN) or a nucleofection apparatus (Lonza) as previously described (Grabham et al., 2007). LysoTracker red (Invitrogen) was added at a 1:2,000 dilution of 1 mM stock solution for 15–30 min to label lysos/LEs and transferred to recording medium for live-cell recordings. 10 kD dextran Alexa Fluor 488 (Invitrogen) was used for an injection marker. Recordings were typically acquired at 1, 5, and 10 min after injection using a 63× oil immersion objective (actual pixel size of 254 nm/pixel) and an EM charge-coupled device camera (C9100-12; Hamamatsu Photonics) attached to an inverted microscope (DM IRBE; Leica). Recordings were generated at 17 frames/s for micoinjection experiments in COS-7 cells and 1 frame/s for RNAi experiments in hippocampal neurons using the MetaMorph stream acquisition function (Molecular Devices).

Motility analysis

A custom-tracking algorithm was used to extract the position of lysosome particles as a function of time (Bremner et al., 2009). A pause is defined as a duration of time with a speed of 100 nm/s or slower. Similar velocity cutoff speed has been used in a previous study (Bremner et al., 2009). A run is defined as the length of travel in the same direction uninterrupted by a pause, and orientation is based on the microtubule-organizing center position versus the location of the cell boundary (Bremner et al., 2009). A motile particle is defined as any particle with displacement $> \sqrt{4Dt}$, where $D = 7.7 \times 10^{-1}$ μm^2/s, as previously described (Bremner et al., 2009). We tracked all spherical particles persisting for ≥50 frames (3 s) and ∼0.254–1.27 μm in size based on fluorescent pixel number (Fig. S3 B) normalized (see next section) to phase-contrast dimensions. All motility analysis is from at least three independent experiments.

Analysis of particle size

Neocortical neurons stained with LysoTracker were monitored live and fixed by addition of 4% PFA to the culture chamber. Phase and fluorescence images of free axonal particles were fitted to an asymmetric 2D

Gaussian shape. The widths reported for each fit for fluorescent and phase-contrast spots were then paired and used to standardize images for the fluorescent particle images to phase-contrast data (Fig. S3 A). The clear correlation between the two sets of spot sizes revealed that the size of fluorescent signals can be used as a proxy of physical particle size. At the same time, the significant uncertainty in individual size assignments makes it challenging to provide finer size separation beyond the large versus small distinction used in this work.

Statistical analysis

For the motility analysis, two-sample comparisons were performed via both Student's *t* test and Wilcoxon rank-sum test. In all other cases, the Student's *t* test alone was used. Statistical significance was inferred for $P < 0.05$ for both tests. All statistical tests were performed using MATLAB (MathWorks), Origin (OriginLab), and Excel (Microsoft) software.

Online supplemental material

Figs. S1 and S2 show characterization of acute dynein, LIS1, and NudE/L inhibition in nonneuronal cells, and Fig. S3 shows examples of lysosome transport in neurons. Videos 1, 2, and 6 show live recordings of lysos/LEs in COS-7 cells injected with 74.1 Ab (Video 1), IgG (Video 2), and DN LIS1 protein (Video 6). Videos 3–5 show high-temporal resolution recordings of lysos/LEs in COS-7 cells at 1 (Video 3), 5 (Video 4), and 10 (Video 5) min after injection. Videos 7–10 show live recordings of lysos/LEs in uninjected (Video 7), 74.1 Ab (Video 8), NudE/L antibody (Video 9), and LIS1 antibody–injected (Video 10) rat cortical neurons. Online supplemental material is available at http://www.jcb.org/cgi/content/full/jcb.201104076/DC1.

We are grateful to Dr. V. Allan for HeLa-M cells and Shahrnaz Kemal for providing primary cultured neurons.

This work was supported by grants GM47434 and HD40182 to R.B. Vallee and GM70676 to S.P. Gross.

Submitted: 14 April 2011
Accepted: 15 September 2011

References

Ally, S., A.G. Larson, K. Barlan, S.E. Rice, and V.I. Gelfand. 2009. Opposite-polarity motors activate one another to trigger cargo transport in live cells. *J. Cell Biol.* 187:1071–1082. http://dx.doi.org/10.1083/jcb.200908075

Barkus, R.V., O. Klyachko, D. Horiuchi, B.J. Dickson, and W.M. Saxton. 2008. Identification of an axonal kinesin-3 motor for fast anterograde vesicle transport that facilitates retrograde transport of neuropeptides. *Mol. Biol. Cell*. 19:274–283. http://dx.doi.org/10.1091/mbc.E07-03-0261

Brady, S.T., K.K. Pfister, and G.S. Bloom. 1990. A monoclonal antibody against kinesin inhibits both anterograde and retrograde fast axonal transport in squid axoplasm. *Proc. Natl. Acad. Sci. USA*. 87:1061–1065. http://dx.doi.org/10.1073/pnas.87.3.1061

Bremner, K.H., J. Scherer, J. Yi, M. Vershinin, S.P. Gross, and R.B. Vallee. 2009. Adenovirus transport via direct interaction of cytoplasmic dynein with the viral capsid hexon subunit. *Cell Host Microbe*. 6:523–535. http://dx.doi.org/10.1016/j.chom.2009.11.006

Culver-Hanlon, T.L., S.A. Lex, A.D. Stephens, N.J. Quintyne, and S.J. King. 2006. A microtubule-binding domain in dynactin increases dynein processivity by skating along microtubules. *Nat. Cell Biol.* 8:264–270. http://dx.doi.org/10.1038/ncb1370

Dujardin, D.L., L.E. Barnhart, S.A. Stehman, E.R. Gomes, G.G. Gundersen, and R.B. Vallee. 2003. A role for cytoplasmic dynein and LIS1 in directed cell movement. *J. Cell Biol.* 163:1205–1211. http://dx.doi.org/10.1083/jcb.200310097

Faulkner, N.E., D.L. Dujardin, C.Y. Tai, K.T. Vaughan, C.B. O'Connell, Y. Wang, and R.B. Vallee. 2000. A role for the lissencephaly gene LIS1 in mitosis and cytoplasmic dynein function. *Nat. Cell Biol.* 2:784–791. http://dx.doi.org/10.1038/35041020

Grabham, P.W., G.E. Seale, M. Bennecib, D.J. Goldberg, and R.B. Vallee. 2007. Cytoplasmic dynein and LIS1 are required for microtubule advance during growth cone remodeling and fast axonal outgrowth. *J. Neurosci.* 27:5823–5834. http://dx.doi.org/10.1523/JNEUROSCI.1135-07.2007

Kardon, J.R., S.L. Reck-Peterson, and R.D. Vale. 2009. Regulation of the processivity and intracellular localization of *Saccharomyces cerevisiae* dynein by dynactin. *Proc. Natl. Acad. Sci. USA*. 106:5669–5674. http://dx.doi.org/10.1073/pnas.0900976106

Kim, H., S.C. Ling, G.C. Rogers, C. Kural, P.R. Selvin, S.L. Rogers, and V.I. Gelfand. 2007. Microtubule binding by dynactin is required for microtubule organization but not cargo transport. *J. Cell Biol.* 176:641–651. http://dx.doi.org/10.1083/jcb.200608128

King, S.J., and T.A. Schroer. 2000. Dynactin increases the processivity of the cytoplasmic dynein motor. *Nat. Cell Biol.* 2:20–24. http://dx.doi.org/10.1038/71338

Lam, C., M.A. Vergnolle, L. Thorpe, P.G. Woodman, and V.J. Allan. 2010. Functional interplay between LIS1, NDE1 and NDEL1 in dynein-dependent organelle positioning. *J. Cell Sci.* 123:202–212. http://dx.doi.org/10.1242/jcs.059337

Martin, M., S.J. Iyadurai, A. Gassman, J.G. Gindhart Jr., T.S. Hays, and W.M. Saxton. 1999. Cytoplasmic dynein, the dynactin complex, and kinesin are interdependent and essential for fast axonal transport. *Mol. Biol. Cell*. 10:3717–3728.

McKenney, R.J., M. Vershinin, A. Kunwar, R.B. Vallee, and S.P. Gross. 2010. LIS1 and NudE induce a persistent dynein force-producing state. *Cell*. 141:304–314. http://dx.doi.org/10.1016/j.cell.2010.02.035

McKenney, R.J., S.J. Weil, J. Scherer, and R.B. Vallee. 2011. Mutually exclusive cytoplasmic dynein regulation by nude-LIS1 and dynactin. *J. Biol. Chem.* In press.

Müller, M.J., S. Klumpp, and R. Lipowsky. 2008. Tug-of-war as a cooperative mechanism for bidirectional cargo transport by molecular motors. *Proc. Natl. Acad. Sci. USA*. 105:4609–4614. http://dx.doi.org/10.1073/pnas.0706825105

Ori-McKenney, K.M., J. Xu, S.P. Gross, and R.B. Vallee. 2010. A cytoplasmic dynein tail mutation impairs motor processivity. *Nat. Cell Biol.* 12:1228–1234. http://dx.doi.org/10.1038/ncb2127

Pilling, A.D., D. Horiuchi, C.M. Lively, and W.M. Saxton. 2006. Kinesin-1 and Dynein are the primary motors for fast transport of mitochondria in *Drosophila* motor axons. *Mol. Biol. Cell*. 17:2057–2068. http://dx.doi.org/10.1091/mbc.E05-06-0526

Ross, J.L., K. Wallace, H. Shuman, Y.E. Goldman, and E.L. Holzbaur. 2006. Processive bidirectional motion of dynein-dynactin complexes in vitro. *Nat. Cell Biol.* 8:562–570. http://dx.doi.org/10.1038/ncb1421

Shu, T., R. Ayala, M.D. Nguyen, Z. Xie, J.G. Gleeson, and L.H. Tsai. 2004. Ndel1 operates in a common pathway with LIS1 and cytoplasmic dynein to regulate cortical neuronal positioning. *Neuron*. 44:263–277. http://dx.doi.org/10.1016/j.neuron.2004.09.030

Shubeita, G.T., S.L. Tran, J. Xu, M. Vershinin, S. Cermelli, S.L. Cotton, M.A. Welte, and S.P. Gross. 2008. Consequences of motor copy number on the intracellular transport of kinesin-1-driven lipid droplets. *Cell*. 135:1098–1107. http://dx.doi.org/10.1016/j.cell.2008.10.021

Siller, K.H., M. Serr, R. Steward, T.S. Hays, and C.Q. Doe. 2005. Live imaging of *Drosophila* brain neuroblasts reveals a role for Lis1/dynactin in spindle assembly and mitotic checkpoint control. *Mol. Biol. Cell*. 16:5127–5140. http://dx.doi.org/10.1091/mbc.E05-04-0338

Smith, D.S., M. Niethammer, R. Ayala, Y. Zhou, M.J. Gambello, A. Wynshaw-Boris, and L.H. Tsai. 2000. Regulation of cytoplasmic dynein behaviour and microtubule organization by mammalian Lis1. *Nat. Cell Biol.* 2:767–775. http://dx.doi.org/10.1038/35041000

Song, A.H., D. Wang, G. Chen, Y. Li, J. Luo, S. Duan, and M.M. Poo. 2009. A selective filter for cytoplasmic transport at the axon initial segment. *Cell*. 136:1148–1160. http://dx.doi.org/10.1016/j.cell.2009.01.016

Soppina, V., A.K. Rai, A.J. Ramaiya, P. Barak, and R. Mallik. 2009. Tug-of-war between dissimilar teams of microtubule motors regulates transport and fission of endosomes. *Proc. Natl. Acad. Sci. USA*. 106:19381–19386. http://dx.doi.org/10.1073/pnas.0906524106

Stehman, S.A., Y. Chen, R.J. McKenney, and R.B. Vallee. 2007. NudE and NudEL are required for mitotic progression and are involved in dynein recruitment to kinetochores. *J. Cell Biol.* 178:583–594. http://dx.doi.org/10.1083/jcb.200610112

Tai, C.Y., D.L. Dujardin, N.E. Faulkner, and R.B. Vallee. 2002. Role of dynein, dynactin, and CLIP-170 interactions in LIS1 kinetochore function. *J. Cell Biol.* 156:959–968. http://dx.doi.org/10.1083/jcb.200109046

Tanaka, T., F.F. Serneo, C. Higgins, M.J. Gambello, A. Wynshaw-Boris, and J.G. Gleeson. 2004. Lis1 and doublecortin function with dynein to mediate coupling of the nucleus to the centrosome in neuronal migration. *J. Cell Biol.* 165:709–721. http://dx.doi.org/10.1083/jcb.200309025

Tsai, J.W., Y. Chen, A.R. Kriegstein, and R.B. Vallee. 2005. LIS1 RNA interference blocks neural stem cell division, morphogenesis, and motility at multiple stages. *J. Cell Biol.* 170:935–945. http://dx.doi.org/10.1083/jcb.200505166

Tsai, J.W., K.H. Bremner, and R.B. Vallee. 2007. Dual subcellular roles for LIS1 and dynein in radial neuronal migration in live brain tissue. *Nat. Neurosci.* 10:970–979. http://dx.doi.org/10.1038/nn1934

Tsai, J.W., W.N. Lian, S. Kemal, A.R. Kriegstein, and R.B. Vallee. 2010. Kinesin 3 and cytoplasmic dynein mediate interkinetic nuclear migration in neural stem cells. *Nat. Neurosci.* 13:1463–1471. http://dx.doi.org/10.1038/nn.2665

Uchida, A., N.H. Alami, and A. Brown. 2009. Tight functional coupling of kinesin-1A and dynein motors in the bidirectional transport of neurofilaments. *Mol. Biol. Cell*. 20:4997–5006. http://dx.doi.org/10.1091/mbc.E09-04-0304

Vergnolle, M.A., and S.S. Taylor. 2007. Cenp-F links kinetochores to Ndel1/Nde1/Lis1/dynein microtubule motor complexes. *Curr. Biol.* 17:1173–1179. http://dx.doi.org/10.1016/j.cub.2007.05.077

Waterman-Storer, C.M., S.B. Karki, S.A. Kuznetsov, J.S. Tabb, D.G. Weiss, G.M. Langford, and E.L. Holzbaur. 1997. The interaction between cytoplasmic dynein and dynactin is required for fast axonal transport. *Proc. Natl. Acad. Sci. USA*. 94:12180–12185. http://dx.doi.org/10.1073/pnas.94.22.12180

Zhang, Q., F. Wang, J. Cao, Y. Shen, Q. Huang, L. Bao, and X. Zhu. 2009. Nudel promotes axonal lysosome clearance and endo-lysosome formation via dynein-mediated transport. *Traffic*. 10:1337–1349. http://dx.doi.org/10.1111/j.1600-0854.2009.00945.x

Zhang, J., L. Zhuang, Y. Lee, J.F. Abenza, M.A. Peñalva, and X. Xiang. 2010. The microtubule plus-end localization of *Aspergillus* dynein is important for dynein-early-endosome interaction but not for dynein ATPase activation. *J. Cell Sci.* 123:3596–3604. http://dx.doi.org/10.1242/jcs.075259